Nanoscale

High-Performance Solar-Blind SnO2 Nanowire Photodetectors Assembled using Optical Tweezers

Journal:	*Nanoscale*
Manuscript ID	NR-ART-09-2018-007382.R2
Article Type:	Paper
Date Submitted by the Author:	29-Nov-2018

Complete List of Authors:	Yan, Jianwei ; Institute of Super-microstructure and Ultrafast Process in Advanced Materials (ISUPAM), School of Physics and Electronics, Central South University Chen, Yang; Institute of Super-microstructure and Ultrafast Process in Advanced Materials (ISUPAM), School of Physics and Electronics, Central South University Wang, Xiaowu; Institute of Super-microstructure and Ultrafast Process in Advanced Materials (ISUPAM), School of Physics and Electronics, Central South University Fu, Ying ; Institute of Super-microstructure and Ultrafast Process in Advanced Materials (ISUPAM), School of Physics and Electronics, Central South University Wang, Juxiang; Institute of Super-microstructure and Ultrafast Process in Advanced Materials (ISUPAM), School of Physics and Electronics, Central South University Sun, Jia; Institute of Super-microstructure and Ultrafast Process in Advanced Materials (ISUPAM), School of Physics and Electronics, Central South University Dai, Guozhang; Hunan Key Laboratory for Super-microstructure and Ultrafast Process, epartment of Physics Science and Electronics Tao, Shaohua; Institute of Super-microstructure and Ultrafast Process in Advanced Materials (ISUPAM), School of Physics and Electronics, Central South University Gao, Yongli; Central South University,

High-Performance Solar-Blind SnO_2 Nanowire Photodetectors Assembled using Optical Tweezers

Jianwei Yan,[1,2] Yang Chen,[1] Xiaowu Wang,[1] Ying Fu,[1] Juxiang Wang,[1] Jia Sun, [1]* Guozhang Dai,[2]* Shaohua Tao,[1]* and Yongli Gao, [1,3]

[1]Hunan Key Laboratory for Super Microstructure and Ultrafast Process, School of Physics and Electronics, Central South University, Changsha, Hunan 410083, P. R. China

[2] Department of Applied Physics, School of Physics and Electronics, Central South University, Changsha 410083, Hunan, China

[3]Department of Physics and Astronomy, University of Rochester, Rochester, NY 14627, USA

J. Yan and Y. Chen contributed equally to this work.

Corresponding Author:

J. Sun (*E-mail: jiasun@csu.edu.cn); G. Dai (*E-mail: gzdai2011@csu.edu.cn); S. Tao (*E-mail: eshtao@csu.edu.cn).

ABSTRACT:

One-dimensional semiconducting SnO_2 nanowires with wide bandgaps are promising candidates to build many important optoelectronic devices. Because building these devices involves the assembly of nanowires into complex structures, manipulation of the active materials needs to be done with high spatial precision. In this paper, an optical tweezer system, comprising a spatial light-modulator, a microscope, and optical elements, is used to individually trap, transfer, and assemble SnO_2 nanowires into two-terminal photodetectors in a liquid environment. After the assembly using optical trapping, the two ends of the SnO_2 nanowire photodetectors, which are connected with the electrodes, were further stabilized using a focused laser. During exposure to 275 nm deep-ultraviolet light, the as-assembled photodetectors show a high I_{ph}/I_{dark} ratio of 2.99×10^5, a large responsivity of 4.3×10^4 A/W, an excellent external quantum efficiency of 1.94×10^5, and a high detectivity of 2.32×10^{13} Jones. The photoresponse-speed of the devices could be improved further using passivation with a polymer. The rise and decay times are about 60 ms and 100 ms, respectively. As a result of this study, we can confirm that non-contact optical trapping can enable the construction of nanowire architectures for optoelectronic, bioelectronic, and other devices.

Keywords: optical tweezers; SnO_2 nanowire; solar-blind; photodetector.

INTRODUCTION

One-dimensional (1D) semiconducting nanowires are promising candidates to fabricate both nano- and bio-electronic components because of their high carrier-mobility, excellent optoelectronic characteristics, and size-dependent physical properties.[1-5] Although patterning of nanowire devices can be performed using traditional microfabrication techniques (such as photolithography and electron-beam lithography), current technologies may limit significant future advances.[6-9] In recent years, some special methods have been used to fabricate nanoscale devices by connecting the electrodes with nanowires. For example, it was discovered that a single carbon nanotube can be placed on two electrodes using alternating-current dielectrophoresis.[10] In addition, an individual semiconducting single-arm carbon nanotube can be placed on two electrodes using floating-potential dielectrophoresis.[11] Nanowires can also be assembled on two electrodes with the help of convective flow, generated by efficient heating of the nanoparticles with high absorption-efficiency.[12] Substantial effort was also put into the exploitation of different methods to assemble 1D nanomaterials on different substrates.[7]

Recently, due to the development of the optical trapping techniques, optical tweezers have been used in optics and other related areas.[13-16] For example, optical tweezers were used to (controllably) move gold nanowires,[17] construct reconfigurable microenvironments for biomedical studies,[18] and to study the biological processes of both protein folding and unfolding.[19] Moreover, the reconstructed beam can also move particles along a designed line produced by a computer-generated hologram,[20] and a fractal zone plate beam can manipulate multiple particles on different planes simultaneously.[21] Furthermore, optical tweezers were utilized to manipulate different types of nanowires to realize special functions or to discover specific physical phenomena. For example, a linearly polarized Bessel beam was employed to capture a single silver nanowire.[22] In addition, the gradient force of the plasmonic optical tweezers in the metal plane was used to capture ZnO nanowires.[23] The position sensor and acousto-optic switch can calibrate the position of nanowires relative to the sample stage of optical tweezers. To study the optical-capturing characteristics of InP nanowires, a single InP semiconductor nanowire, which was trapped by optical tweezers, was used to produce both nonlinear optical excitation and two-photon absorption.[24, 25] Holographic optical tweezers were also helpful to scan the captured InP nanowires in the direction of light and record the luminescence

characteristic.[26] Semiconductor nanowires can be translated, rotated, cut, fused, and organized into nontrivial structures with the help of holographic optical traps.[26] Trapped nanowires with a high aspect-ratio were assembled into an arbitrary structure in a liquid environment, using the gradient force of an infrared light.[6] However, the manipulation of nanowires by optical tweezers for optoelectronics devices has rarely been reported.

In this paper, an optical tweezer system comprising a spatial light modulator, microscope, and optical elements, is used to assemble SnO_2 nanowires in a liquid. The optical trapped nanowires can be accurately assembled into two patterned-electrodes to produce a photodetector. We describe, in detail, both the fabrication method and related technical problems. The device performance of the photodetectors is also studied. Our results demonstrate that non-contact optical trapping enables the construction of nanowire architectures suitable for optoelectronic and bioelectronics devices.

RESULTS AND DISCUSSION

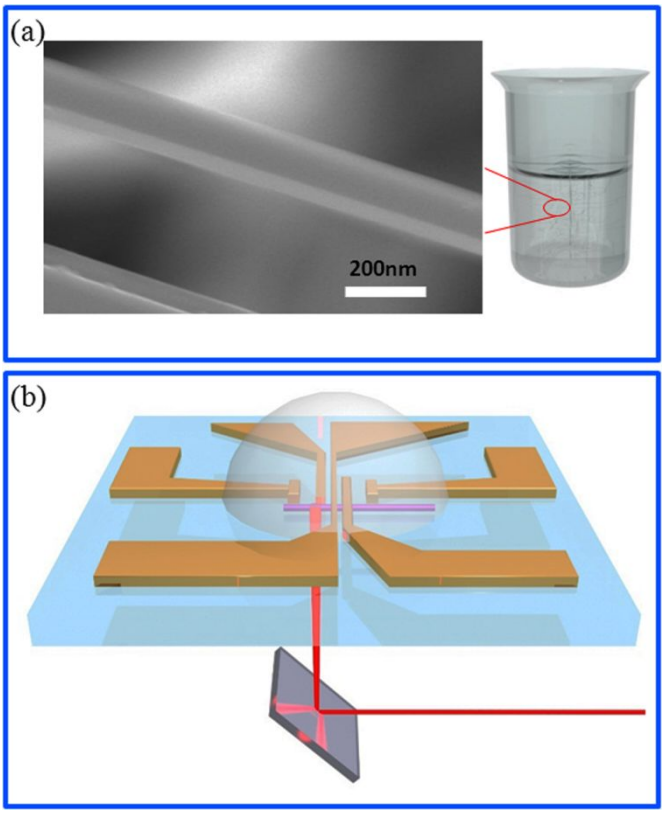

Figure1. (a) High magnification SEM images of individual SnO_2 nanowires, and schematic of nanowires dispersed in alcohol. (b) Schematic of the manipulation of a nanowire using optical trapping on a glass substrate.

The high-quality and single-crystalline SnO_2 nanowires were synthesized using chemical vapor deposition, which usually follows a vapor-liquid-solid growth mechanism. The morphology of as-synthesized SnO_2

nanowires was examined. As shown in **Fig. 1(a)**, a typical high-resolution scanning electron microscopy (SEM) image indicates that the nanowires have a very smooth surface, with little variation in shape along the wire's axis. Generally, the SnO_2 nanowires show a diameter distribution of 50 to 200 nm and a length of tens of micrometers (**Fig. S1**). In order to assemble SnO_2 nanowires as nanoscale photodetectors using optical trapping, the collected SnO_2 nanowires were dispersed in a deionized water/alcohol solution. **Fig. 1(b)** shows a schematic image of SnO_2 nanowires, which were assembled between, two electrodes using optical trapping. The Cr/Ti electrodes were pre-patterned using photolithography which was deposited on glass substrates. The photolithographic fabrication steps are illustrated in **Fig. S2**. Trapping experiments were performed in a purpose-built optical-tweezers system. The refractive index of SnO_2 (bulk) is about 2.[27] It is also reported that SnO_2 nanowires prepared using a vapor–liquid–solid mechanism is a wide-bandgap semiconductor with a bandgap of 3.74eV.[28] In our optical-trapping experiment, a 532 nm laser was used. Thus, any absorption would be very small. In addition, during the optical trapping step, the laser was focused onto the end of SnO_2 nanowire. Within the channel region, the laser power should be very low, and the photodamage to the nanostructure of SnO_2 nanowires would be negligible. The laser-light was introduced through the rear-side of the glass substrate to trap the SnO_2 nanowires. Once the nanowire was trapped in a stable manner, manipulation was performed with a home-built translation stage. When the translation stage was adjusted, the glass substrate could move but the position of the focal spot did not change. However, the SnO_2 nanowire can be moved to the focal point thanks to the force generated by the intensity-gradient. In other words, the movement of the SnO_2 nanowire can be controlled by adjusting the translation stage appropriately.

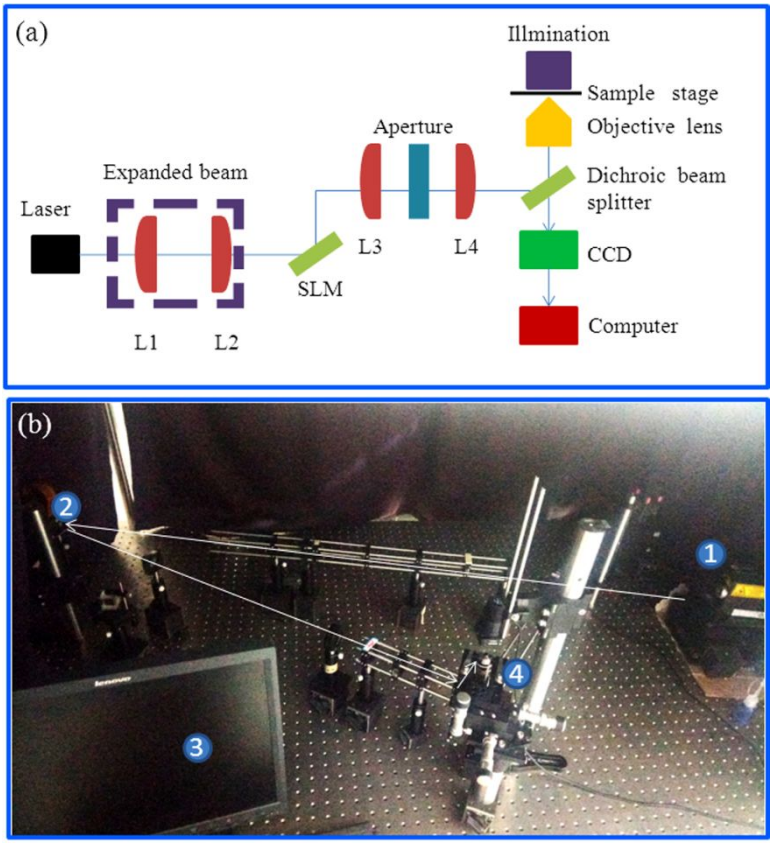

Figure 2. (a) Schematic picture of the optical tweezers platform. (b) Photograph of the optical tweezer platform.

Fig. 2(a) and **2(b)** show a schematic and photograph of the optical tweezer platform. In Fig. 2(b), the solid lines show the propagation path of the laser beam. The labels 1, 2, 3, and 4 mark the diode-pumped laser (Coherent, Genesis MX532-1000 STM, λ=532 nm, 1 W), spatial light modulator (SLM, Boulder Nonlinear System, model P512-532 nm, 512 ×512 pixels, 15 μm×15 μm /pixel, multilevel phases, reflective), computer screen, and sample stage of the microscope. The beam propagates as follows: firstly, the beam is emitted from the laser and passes through the beam-expanding system, which consists of L1, with a focal length of 30 mm, and L2, with a focal length of 300 mm. Then, the beam is deflected by the grating in the SLM. The beam is then condensed by the inverted telescope system, which consists of L3, with the focal length of 250 mm, and L4, with the focal length of 50 mm. The beam is further focused using a 100×oil-immersion objective lens (Olympus, N.A. 1.3) of an inverted microscope. Finally, the focal spot of the objective lens captured by a charge-coupled device (CCD) can be displayed on a computer screen. Based on the optical tweezers platform shown in **Fig. 2**, we will manipulate the nanowires suspended in a deionized water/ alcohol solution.

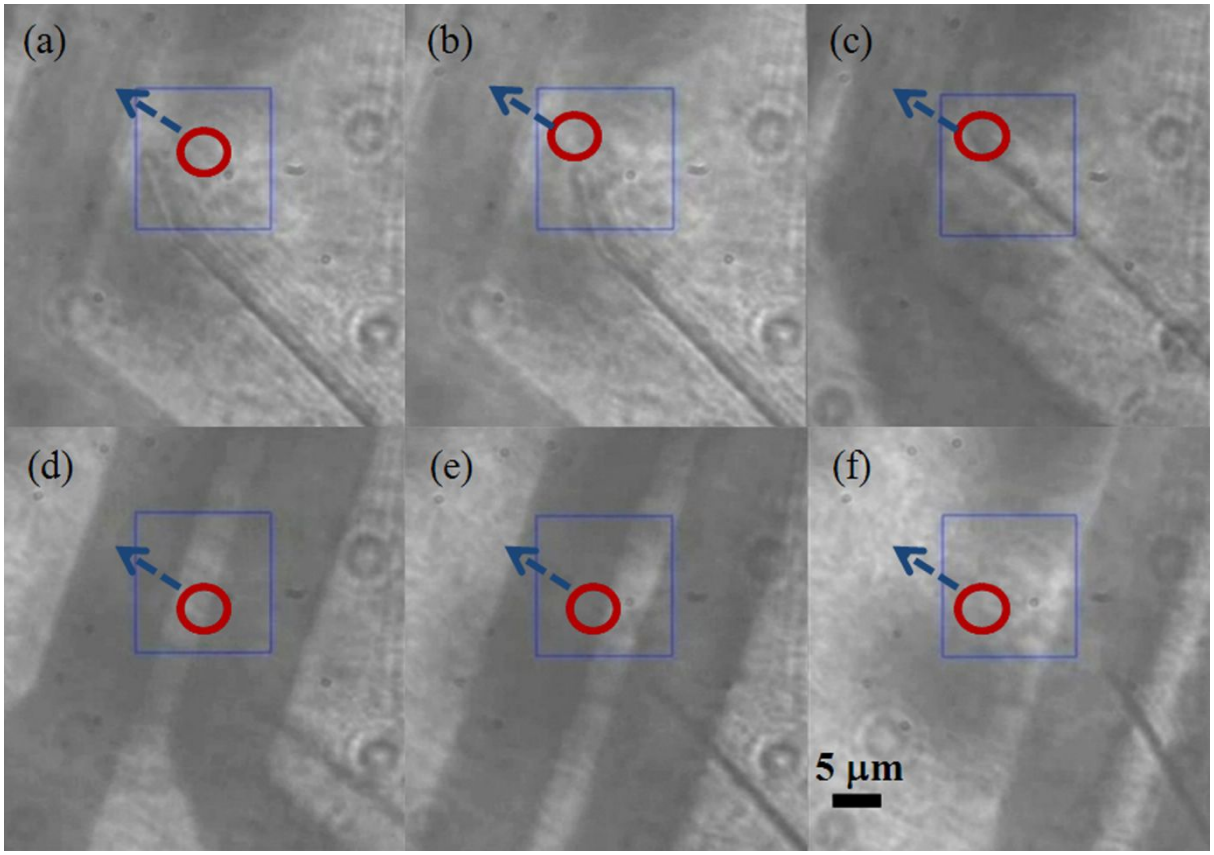

Figure 3. (a)-(f) The CCD-captured frames of a single SnO_2 nanowire that is moved and placed on top of the two electrodes.

Fig. 3 shows the CCD-captured frames, which demonstrate that a single SnO_2 nanowire can be moved sequentially and placed onto the two electrodes. Firstly, the power of the laser was set to 3 mW, and we selected a single SnO_2 nanowire near the electrodes using the CCD. Then, after the laser power gradually increased to 800 mW, one end of the SnO_2 nanowire (close to the focal spot) was trapped due to the force generated by the intensity-gradient. As a result, we were able to gradually move the entire SnO_2 nanowire using the pulling force. Therefore, we could control the movement of the single SnO_2 nanowire and put the SnO_2 nanowire on top of the two electrodes. The squares, circles, and arrows in **Fig.3** mark the focused region of the beam, focal spot, and moving direction of the single SnO_2 nanowire, respectively. It can be observed that the single SnO_2 nanowire was indeed placed on both electrodes using the mechanical movement of the focal spot. Subsequently, the nanowires and the optoelectronic device were dried to enable good cohesive contact between the nanowire and the electrodes using the high-power laser-beam of 1 W. Finally, the single SnO_2 nanowire photodetector was constructed using the optical trapping method. Because the alcohol solution is very volatile, the nanowire-solution dries quickly. While moving SnO_2 nanowire to

the electrodes, using optical tweezers, the laser was continuously focused on the end of nanowires until the solvent dried up. Because the SnO_2 nanowire length exceeds tens of micrometers, the nanowires are heavy and stable during the drying process. Furthermore, the length of the SnO_2 nanowires is far greater than the channel size. Even if the SnO_2 nanowires had moved slightly during the drying process, it would not have affected the assembly of the devices using optical tweezers. A video showing more details of the manipulation of the nanowires via optical tweezers can be found in the **supplementary material**. The SEM image of the SnO_2 nanowire photodetector, assembled with optical tweezers, is shown in **Fig. S3**. The diameter of the nanowire was measured to be ~40 nm.

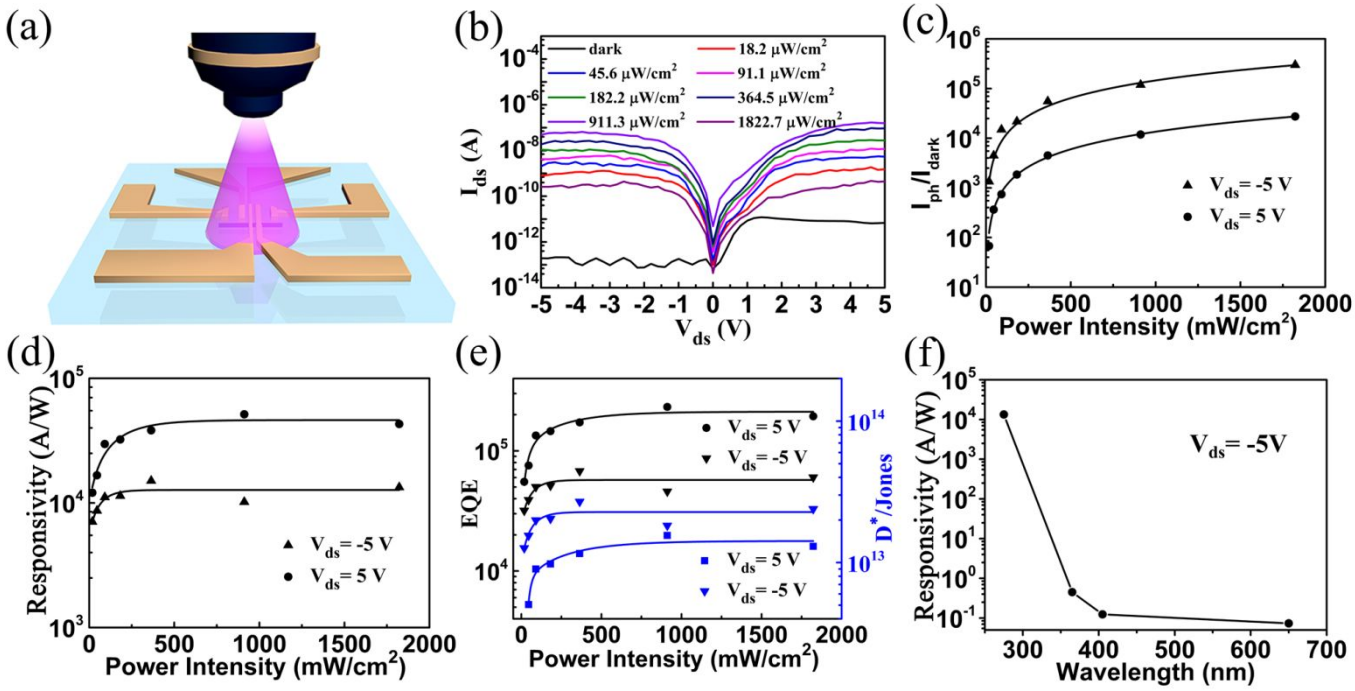

Figure 4. (a) Schematic of the single nanowire photodetector using light illumination. (b) I-V curves for a device under 275 nm laser illumination with various power intensities and in the dark. (c) Light (power) intensity dependent I_{ph}/I_{dark} for the device under 275 nm incident light at a voltage bias of ±5V. (d) Light-intensity-dependent R for 275 nm incident light at voltage bias of ±5V. (e) Light-intensity-dependent EQE and D* for 275 nm incident light at voltage bias of ±5 V. (f) Wavelength-dependent R for the same power intensity of 1822.7 μW/cm².

The optoelectronic properties of a nanowire photodetector, assembled using optical trapping, are investigated in more depth. A schematic image of a photodetector device used for the photo-response measurement for a single SnO_2 nanowire is shown in **Fig. 4(a)**. Monochromatic light-sources with different wavelengths and power densities were shone on the nanowires connected to one pair of Cr/Ti electrodes. The photocurrent was recorded using a two-probe method. The typical I-V characteristics of SnO_2 nanowire photodetectors is shown in **Fig. 4(b)**. These were measured in the dark or under deep-ultraviolet (275 nm)

using different light densities. As indicated by the black line in **Fig. 4(b)**, the devices shows a very low dark-current at -5 V (~10^{-13} A). The dark current in forward bias is slightly enlarged to ~10^{-12} A. The asymmetric I-V curve indicates that a barrier formed between the Ti electrode and the SnO_2 nanowire. For the SnO_2 nanowire, the large surface-to-volume ratio produces surface states due to breaking the lattice periodicity. Because SnO_2 is a typical n-type semiconductor with some oxygen vacancies, a back-to-back Schottky barrier forms aided by Fermi level pinning and surface states or defects. An asymmetric current between forward bias and reverse bias may be due to the asymmetric Schottky barrier. The photocurrent, measured under light irradiation, show an clear current change, which indicates that light is also used to photo-generate carriers. When the light power density changed from 18.2 μW/cm^2 to 1822.7 μW/cm^2, the photocurrents increased significantly. The photocurrents (light power density: 1822.7 μW/cm^2) at –5 V and 5 V are about 4.877×10^{-8} A and 1.57×10^{-7} A, respectively. The I_{ph}/I_{dark} ratio is an important parameter to evaluate the performance of a photodetector. It reveals the sensitivity of the device for a given irradiation. **Fig. 4(c)** shows the light intensity dependency of I_{ph}/I_{dark} to 275 nm light at a bias of ±5 V for the SnO_2 nanowire photodetectors. It is clear that I_{ph}/I_{dark} increases significantly when the light power density increases, and it would not change much more if the light power density exceeds 1000 μW/cm^2. The maximal I_{ph}/I_{dark} ratios at -5 V and 5 V are calculated to be 2.99×10^5 and 2.74×10^4, respectively.

In order to indicate the photocurrent response, two important parameters (responsivity (R), external quantum efficiency (EQE)) are usually used to evaluate the photoelectric conversion of a photodetector.[29-32] R is defined as the ratio of the photocurrent to the incident optical power for the active area of a nanowire photodetector. This can be expressed as $R=(I_{ph}-I_{dark})/PS$, where P is the light power density, and S is the effective nanowire area. EQE reflects the energy-conversion efficiency from light to electric, which can be calculated as $EQE=Rhv/q$, where hν is the photon energy, and e is the electron charge. The light power density dependent R at 275 nm of the SnO_2 nanowire photodetectors with a voltage bias of ±5V is shown in **Fig. 4(d)**. R rapidly improves when the light power density increases, and then almost saturates. This behavior can be attributed to the saturation of the photocurrent at high light intensity. Under light illumination, the increasing of nanowire's conductance is mainly originated from the following reasons. Firstly, a large number of hole-electron pairs generated by light irradiation are collected by electrodes with

the assistance of external electric field. Secondly, due to the absorbed oxygen at the surface of SnO_2 nanowire, the electrons were trapped in the surface of SnO_2 nanowire, which forms a depletion-layer with low-conductivity. With light irradiation, the photoexcited holes can significantly accelerate the desorption process of oxygen. The width of surface depletion layer is reduced. As the further increasing of light power density, the photo-generated carrier density is improved and the width of depletion layer is narrowed more significantly. This process is equivalent to photo-assisted electron-type electrostatic doping, which significantly increases the electron density in the conduction band and enhances the conductivity of the nanowire. Because of the long relaxation time of charge trapping and detrapping with oxygen to a dynamic equilibrium, the response time of the devices is slow (see Figure 5). In our measurement, we measured the devices with gradually increasing of light power intensity. After one sweep of I-V curve, we then repeat the same measurement with a larger light power density. Due to the long relaxation time, the photo-generated electrons by last sweep are persisted in SnO_2 nanowire channel. After a continuous multiple scanning with increasing light power, high density electrons are accumulated and a significant increasing conductivity of SnO_2 nanowire was observed. Thus, the calculated photoresponsivity is increased with improvement of light intensity. Similar results are observed in other oxide nanowire photodetectors.[33, 34]

When the 275 nm light with a large power density shines onto the device, the number of charge carriers, which are generated by the continuous incident light beam, get saturated and the *R* becomes unaffected by increased light power. When the light power density is 1822.7 $\mu W/cm^2$, the obtained *R* for the device, biased at 5 V, is 4.30×10^4 A/W. This is about three times higher than for the device biased at -5V. The *EQE* and detectivity (*D**) as a function of light power density, with a voltage bias of ±5V, are shown in **Fig. 4(e)**. For the SnO_2 nanowire photodetector, biased at 5V, the *EQE* reaches a maximum of 1.94×10^5, which is about three times larger than for devices operated at -5V. It is known that *D** is the minimum detectable power irradiation. Its value depends on the dark current of the devices. However, *D** at 5V is slightly smaller, which is mainly due to the larger dark current at positive bias. The maximum D* at -5V for the devices is as large as 2.32×10^{13} Jones. These high numbers for I_{ph}/I_{dark}, *R*, *EQE* and *D** indicate a high sensitivity and weak noise of the measured nanowire photodetectors. The device performance of the SnO_2 nanowires, which were fabricated using optical trapping, are comparable to previously published reports about deep-ultraviolet

oxide photodetectors.[34-37]

The photoresponse of the SnO_2 nanowire photodetector as a function of illuminated light wavelength, with an irradiation light intensity of 1822.7 μW/cm^2 at a bias of -5V at room temperature, is shown in **Fig. 4(e)**. The typical I-V curve is shown in **Fig. S4**. The photodetector shows a high R (4.3×10^4 A/W) for deep-ultraviolet light (275 nm). After increasing the wavelength (decreasing the photon energy), R decreases significantly. It can be clearly seen that R at 275 nm is about 5 orders of magnitude higher than for devices measured in the ultraviolet/visible light range. Such a high photoresponse at deep-ultraviolet light indicates that the as-fabricated photodetector has a relatively high spectral selectivity with respect to solar-blind detection.

Important factors that determine the tuneability of a photodetector are the photoresponse speed and reproducibility under light illumination. To evaluate the combined properties of the SnO_2 nanowire photodetector, the time-dependent photocurrent was recorded under 275 nm light irradiation for a operating voltage bias of 5 V. The incident light beam was repeatedly switched between on and off, with a power density of 1822.7 μW/cm^2, as shown in **Fig. 5(a)**. The figure shows that a significant change of the photocurrent occurs during exposure to light. Although the SnO_2 nanowire photodetector fabricated using optical-trapping is very stable, with well reproducible photoresponse characteristics after 6 cycles of light illumination, the switch-on photocurrent responds slowly to light switching. A magnified view (**Fig. 5(b)**) of one cycle of light switching show that the increase and decay times of the SnO_2 nanowire photodetector were 33 s and 85 s. In general, the ultraviolet photoresponse of oxide nanowire materials can be explained using two different mechanisms, which are known as bulk or surface related processes. Previous reports propose that the passivation of the oxide surface using polymers can significantly enhance the ultraviolet photoresponse speed of oxide semiconductor photodetectors. **Fig. 5(c)** and **Fig. 5(d)** show the time-resolved photocurrent curve for a SnO_2 nanowire photodetector passivated with a P(VDF-TrFE) polymer. The change in photocurrent with light-switching, however, reveals different characteristics for the *passivated* SnO_2 nanowire photodetectos. After switching the deep-ultraviolet light-source on, the photocurrent rises sharply and decays quickly after switching the light off. Both rise and decay times of the passivated sample are significantly improved (60 ms and 100 ms, respectively). Compared to the non-coated samples, the

photoresponse-speed improved by at least two orders of magnitude in the P(VDF-TrFE)- passivated SnO_2 nanowire photodetectors. However, there is a different dark current and photocurrent in the nanowire depending on whether P(VDF-TrFE) was used or not. The I_{ph}/I_{dark} ratio for the P(VDF-TrFE)-passivated SnO_2 nanowire device decreased significantly. Our devices were measured in air, and some water molecules or organic components could be contained in the polymer. We found that the minimum current is not at V_{ds} = 0V (**Fig. S5**). This indicates that a leakage current was present after the polymer passivation, which is mainly due to the ion-motion-induced ionic-current or an electrochemical reaction in P(VDF-TrFE).

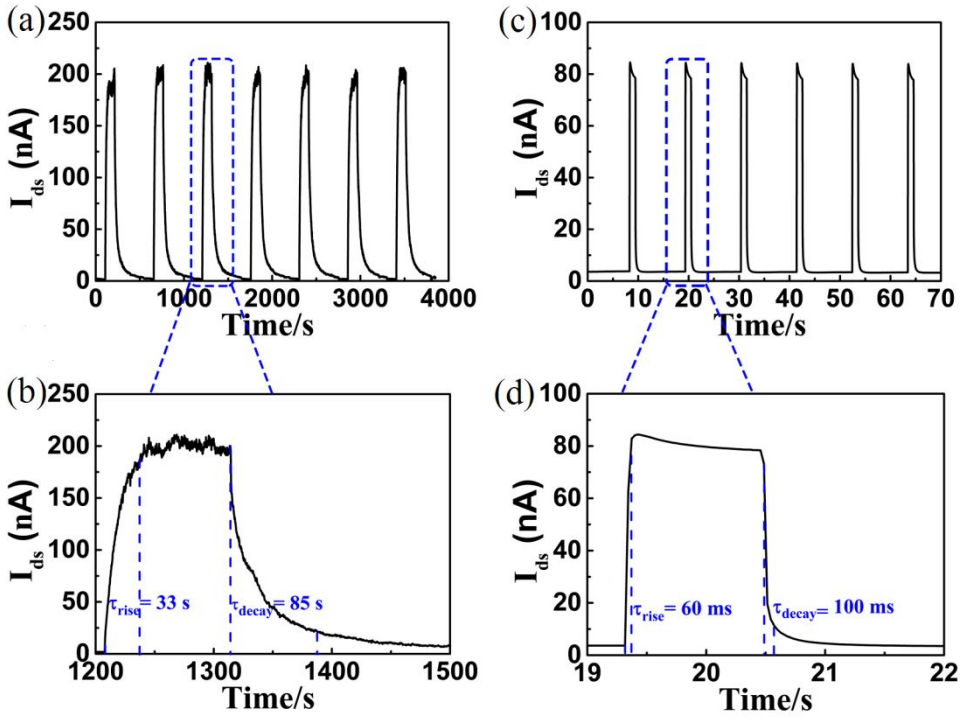

Figure 5. (a)Time-dependent photocurrent curve, recorded by repeatedly turning the light on and off at 5V bias. (b) One cycle of light switching from Fig. 5(a). (c) Time-resolved photocurrent curve for the SnO_2 nanowire photodetector passivated with a P(VDF-TrFE) polymer. (d) Changing photocurrent for light switching during one cycle - data taken from Fig. 5(c).

The mechanism underlying the enhancement of the photoresponse-speed of the P(VDF-TrFE)-passivated SnO_2 nanowire photodetectors is discussed and the corresponding energy-level evolution is shown in **Fig. 6**. It is well-known that the electrical characteristics of metal-oxide nanowires strongly depend on the surrounding environment.[38-40] Oxygen molecules can be absorbed on the nanowire surface, which results in trapped electrons coming from the bulk. Generally, the adsorbed oxygen can capture electrons with an oxygen-ion species [$O_2(g)+e^-=O_2^-(ad)$]. Thus, a low-conductivity depletion-layer forms near the surface of the oxide nanowire, which leads to increased upward surface-band bending (**Fig. 6(a)**). During

deep-ultraviolet light illumination, the chemisorbed oxygen molecules are liberated with the help of photo-generated holes.[40, 41] The electrons are released into the nanowires, which increases the conductivity of the sample (**Fig. 6(b)**). As the deep-ultraviolet light switches off, the electrons and holes recombine to return to the initial state. The oxygen molecules reabsorb onto the surface of nanowires (**Fig. 6(c)**). After the passivation of the SnO_2 nanowire photodetectors, the desorbed oxygen molecules from the nanowire surface concentrates around the host nanowire due to the encapsulation effect of the P(VDF-TrFE) polymer. Because of gas isolation in ambient air, the band structure is nearly flat, as shown in **Fig. 6(d)**. Coating with the polymer can also passivate the electron states of oxide nanowires because of the dangling bonds located at surface.[42-44] Thus, substantially reduced oxygen absorption/desorption allows the photo-generated carriers to move faster, with fewer traps present.

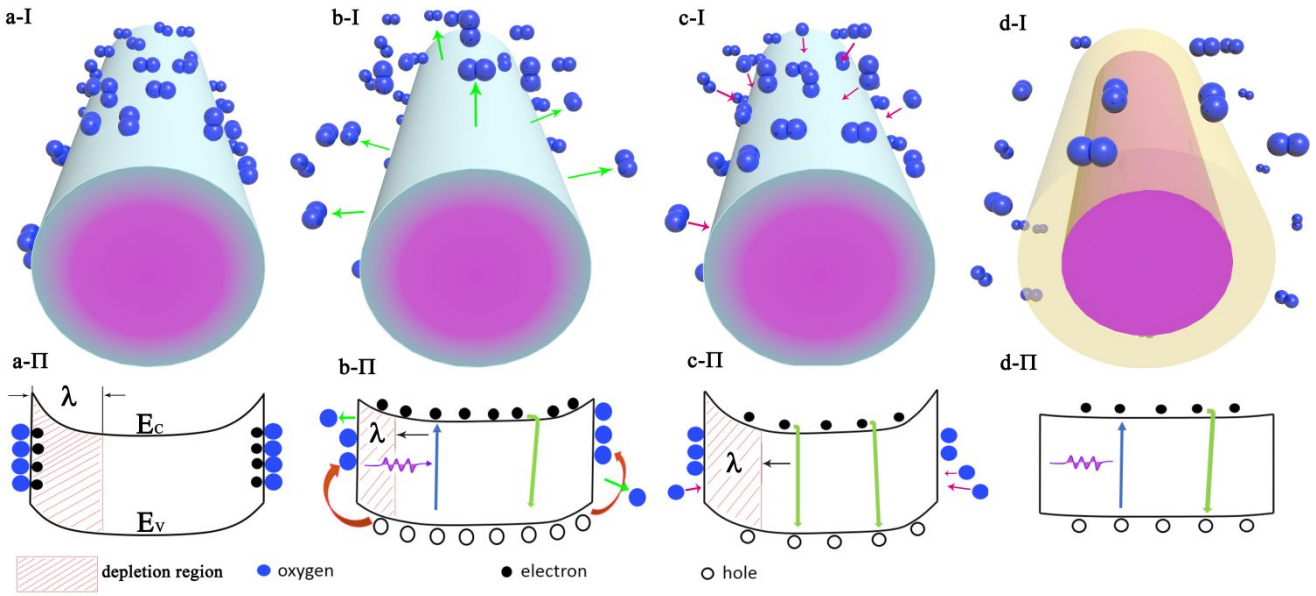

Figure 6. Underlying mechanism for the enhanced photoresponse-speed of the SnO_2 nanowire photodetector with polymer passivation.

CONCLUSION

We have demonstrated the trapping and manipulation of a single SnO_2 nanowire in a liquid environment using an optical-tweezer system on a flat glass-substrate. The optically trapped nanowires can be precisely assembled onto two patterned-electrodes to act as a photodetector. The as-prepared SnO_2 nanowire photodetectors show an excellent solar-blind photodetection performance with a high I_{ph}/I_{dark} ratio of

2.99×10^5, a large R of 4.3×10^4 A/W, a high EQE of 1.94×10^5, and a high D^* of 2.32×10^{13} Jones. Upon passivation of the devices with a polymer, the photoresponse-speed improves significantly, with a rise and decay times of 60 ms and 100 ms, respectively. The results of this study indicate that this novel precise one-dimensional nanowire manipulation method opens new doors for nanoscale optoelectronic and bioelectronic applications.

Experimental

Single-crystalline SnO_2 nanowires were synthesized using oxygen-assisted chemical vapor deposition in a horizontal tube-furnace. A small quartz-tube loaded with high-purity Sn (0.1 g) powder is placed into the heating zone of a furnace. The silicon wafers (110), which were used to collect deposited products, were ultrasonically cleaned for 10 min in acetone and ethanol. A 10-nm-thick Au layer, which was deposited on the silicon wafers, was used as the catalyst to grow the nanowires. Then, the silicon wafers, with the polished surface facing down, were placed on the top of a quartz tube that contains Sn powder. Prior to heating, pure Ar (99.99%) was blown into the horizontal tube at a rate of 80 sccm for 30 min to purge the atmosphere. Then the pressure was decreased to 20 Pa. The central zone was heated to 900 °C in 30 min, while the pressure was maintain at 20 Pa. After 60 min of growth, the furnace was naturally cooled down to room temperature. Patterned electrodes (Cr/Ti (10 nm/60 nm)), with a channel length of ~4 μm on the glass substrate, were fabricated using a standard photolithography process. Firstly, the glass substrates were covered with a photoresist via spin coating and annealing (100 °C, 20 min). Secondly, the substrate with photoresist was exposed to ultraviolet light using a pre-patterned mask. Thirdly, the exposed photoresist was removed using a suitable developer. Then, metal electrodes were deposited using magnetron sputtering under low vacuum (5×10^{-4} Pa). Finally, any unused metal residues on the photoresist were washed away using acetone, which completes the patterning of the electrodes on the glass substrate.

The as-prepared SnO_2 nanowire was dispersed in a deionized water/alcohol (volume ratio = 4:1) solution. One drop of nanowire solution was dropped onto the patterned electrodes. The grating, which was loaded on the SLM, can be used to deflect the focused laser beam to the desired location in the sample stage. The glass substrate with the etched electrodes was placed on the translation stage. The power of the laser was set to 3 mW, and a single SnO_2 nanowire around the electrodes was selected. The manipulation of the

nanowire was monitored with a CCD. The laser power gradually increased to 800 mW, and the SnO_2 nanowire was placed on both electrodes using the pulling force generated by adjusting the translation stage. In order to improve the contacts, the intersection of SnO_2 nanowire and electrodes was dried using the laser beam (with 1W power).

The photodetection characteristics of the as-prepared individual SnO_2 nanowire devices were measured using a semiconductor parameter-analyzer (Keithley 4200-SCS) in a black box. The lasers, driven by a source-meter unit (Keithley 4200-SCS), vertically illuminated the device at a distance of 1.5 cm. All data were recorded in air with a relative humidity of about 30%.

Acknowledgement

This work was supported by the National Natural Science Foundation of China (61306085, 11674401, 11334014) and the Hunan Provincial Natural Science Foundation of China (2018JJ3679). Y. G. acknowledges support by National Science Foundation CBET-1437656. Y. C. acknowledges support by the Fundamental Research Funds for the Central Universities of Central South University (2018zzts334).

REFERENCES

1 R. Yan, D. Gargas and P. Yang, *Nature Photonics*, 2009, **3**, 569-576.
2 E. N. Dattoli, Q. Wan, W. Guo, Y. Chen, X. Pan and W. Lu, *Nano Lett.*, 2007, **7**, 2463-2469.
3 X. Liu, X. Liu, J. Wang, C. Liao, X. Xiao, S. Guo, C. Jiang, Z. Fan, T. Wang, X. Chen, W. Lu, W. Hu and L. Liao, *Adv. Mater.*, 2014, **26**, 7399-7404.
4 L. Hu, J. Yan, M. Liao, L. Wu and X. Fang, *Small*, 2011, **7**, 1012-1017.
5 G. Gou, G. Dai, C. Qian, Y. Liu, Y. Fu, Z. Tian, Y. He, L. Kong, J. Yang, J. Sun and Y. Gao, *Nanoscale*, 2016, **8**, 14580-14586.
6 P. J. Pauzauskie, A. Radenovic, E. Trepagnier, H. Shroff, P. Yang and J. Liphardt, *Nat Mater*, 2006, **5**, 97-101.
7 Y. Z. Long, M. Yu, B. Sun, C. Z. Gu and Z. Fan, *Chem. Soc. Rev.*, 2012, **41**, 4560-4580.
8 J. Sun, Q. Tang, A. Lu, X. Jiang and Q. Wan, *Nanotechnology*, 2009, **20**, 255202.
9 S.-W. Lee, G. Jo, T. Lee and Y.-G. Lee, *Opt. Express*, 2009, **17**, 17491-17501.
10 R. Krupke, F. Hennrich, H. B. Weber, M. M. Kappes and H. Lohneysen, *Nano Lett.*, 2003, **3**, 1019-1023.
11 L. Dong, V. Chirayos, J. Bush, J. Jiao, V. M. Dubin, Chebian, Ramanan V., Y. Ono, J. F. Conley, Jr. and B. D. Ulrich, *J. Phys. Chem. B*, 2005, **109**, 13148-13153.
12 B. K. Wilson, M. Hegg, X. Miao, G. Cao and L. Y. Lin, *Opt. Express*, 2008, **16**, 17276-17281.
13 J. E. Curtis, B. A. Koss and D. G. Grier, *Opt. Commun.*, 2002, **207**, 169-175.
14 S. Cheng, S. Tao, C. Zhou and L. Wu, *Journal of Optics*, 2015, **17**, 105613.
15 X. Wang, S. Chen, M. Kong, Z. Wang, K. D. Costa, R. A. Li and D. Sun, *Lab Chip*, 2011, **11**, 3656-3662.
16 S. Cheng, S. Tao, X. Zhang and W. Ma, *IEEE Photonics Journal*, 2016, **8**, 1-7.
17 Y. Zhang, J. Wang, J. Shen, Z. Man, W. Shi, C. Min, G. Yuan, S. Zhu, H. P. Urbach and X. Yuan, *Nano Lett.*, 2014, **14**, 6430-6436.
18 P. J. John Rodrigo, L. Kelemen, D. Palima, C. A. Alonzo, P. O. Ormos and J. Glückstad1, *Opt. Express*, 2009, **17**, 6578-6583.
19 D. Collin, F. Ritort, C. Jarzynski, S. B. Smith, I. Tinoco, Jr. and C. Bustamante, *Nature*, 2005, **437**, 231-234.
20 S. Tao and W. Yu, *Opt. Express*, 2015, **23**, 1052-1062.
21 S. Cheng, X. Zhang, W. Ma and S. Tao, *Sci. Rep.*, 2016, **6**, 34492.
22 Z. Yan, J. E. Jureller, J. Sweet, M. J. Guffey, M. Pelton and N. F. Scherer, *Nano Lett.*, 2012, **12**, 5155-5161.
23 L. Zhang, X. Dou, C. Min, Y. Zhang, L. Du, Z. Xie, J. Shen, Y. Zeng and X. Yuan, *Nanoscale*, 2016, **8**, 9756-9763.
24 P. J. Reece, W. J. Toe, F. Wang, S. Paiman, Q. Gao, H. H. Tan and C. Jagadish, *Nano Lett.*, 2011, **11**, 2375-2381.
25 F. Wang, P. J. Reece, S. Paiman, Q. Gao, H. H. Tan and C. Jagadish, *Nano Lett.*, 2011, **11**, 4149-4153.
26 R. Agarwal, K. Ladavac, Y. Roichman, G. Yu, C. M. Lieber and D. G. Grier, *Opt. Express*, 2005, **13**, 8906-8912.
27 S. H. Mohamed, *J. Alloys Compd.*, 2012, **510**, 119-124.
28 S. Luo, J. Fan, W. Liu, M. Zhang, Z. Song, C. Lin, X. Wu and P. K. Chu, *Nanotechnology*, 2006, **17**, 1695-1699.
29 F. Teng, K. Hu, W. Ouyang and X. Fang, *Adv. Mater.*, 2018, **30**, 1706262.
30 H. Xia, S. Tong, C. Zhang, C. Wang, J. Sun, J. He, J. Zhang, Y. Gao and J. Yang, *Appl. Phys. Lett.*, 2018, **112**, 233301.
31 C. Qian, J. Sun, L.-A. Kong, G. Gou, M. Zhu, Y. Yuan, H. Huang, Y. Gao and J. Yang, *Adv. Funct. Mater.*, 2017, **27**, 1604933.
32 S. Tong, H. Wu, C. Zhang, S. Li, C. Wang, J. Shen, S. Xiao, J. He, J. Yang, J. Sun and Y. Gao, *Org. Electron.*, 2017, **49**, 347-354.
33 W. Feng, X. Wang, J. Zhang, L. Wang, W. Zheng, P. Hu, W. Cao and B. Yang, *Journal of Mater Chem C*, 2014, **2**, 3254.
34 M. Chen, B. Zhao, G. Hu, X. Fang, H. Wang, L. Wang, J. Luo, X. Han, X. Wang, C. Pan and Z. L. Wang, *Adv. Funct. Mater.*, 2018, **28**, 1706379.
35 L. Li, P. S. Lee, C. Yan, T. Zhai, X. Fang, M. Liao, Y. Koide, Y. Bando and D. Golberg, *Adv. Mater.*, 2010, **22**, 5145-5149.
36 B. Zhao, F. Wang, H. Chen, Y. Wang, M. Jiang, X. Fang and D. Zhao, *Nano Lett.*, 2015, **15**, 3988-3993.
37 X. Zhou, Q. Zhang, L. Gan, X. Li, H. Li, Y. Zhang, D. Golberg and T. Zhai, *Adv. Funct. Mater.*, 2016, **26**, 704-712.
38 B. J. Coppa, C. C. Fulton, P. J. Hartlieb, R. F. Davis, B. J. Rodriguez, B. J. Shields and R. J. Nemanich, *J. Appl. Phys.*, 2004, **95**, 5856-5864.

39 M. W. Allen and S. M. Durbin, *Appl. Phys. Lett.*, 2008, **92**, 122110.

40 C.-Y. Chen, J. Retamal, I.-W. Wu, D.-H. Lien, M.-W. Chen, Y. Ding, Y.-L. Chueh, C.-I. Wu and J.-H. He, *ACS Nano*, 2012, **6**, 9366-9372.

41 S. Bayan, S. K. Mishra, B. Satpati and P. Chakraborty, *Mater. Sci. Semicond. Process.*, 2014, **24**, 200-207.

42 D. P. Joan, J.-D. Roman, H.-R. Francisco, F.-R. Luis, A. Teresa, C. Albert, R.-R. Albert, C. Albert, R. M. Joan, B. Sven and M. Sanjay, *J. Phys. Chem. C*, 2008, **112**, 14639-14644.

43 W.-K. Hong, J. I. Sohn, D.-K. Hwang, S.-S. Kwon, G. Jo, S. Song, S.-M. Kim, H.-J. Ko, S.-J. Park, M. E. Welland and T. Lee, *Nano Lett.*, 2008, **8**, 950-956.

44 J. D. Prades, F. Hernandez-Ramirez, R. Jimenez-Diaz, M. Manzanares, T. Andreu, A. Cirera, A. Romano-Rodriguez and J. R. Morante, *Nanotechnology*, 2008, **19**, 465501.

A table of contents entry

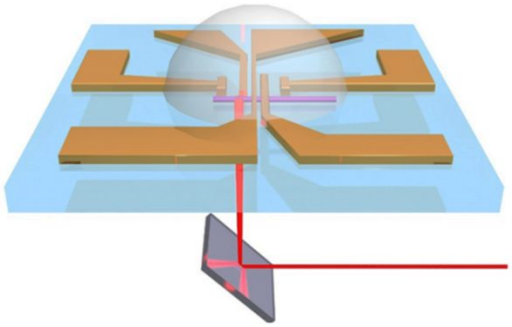

An optical tweezer system is used to individually trap, transfer, and assemble SnO_2 nanowires into two-terminal photodetectors in a liquid environment.